Skeletal Virtual Tube Generation for Urban UAV Swarm Navigation

Xunhua Dai[1] and Yuting Liao[2]

***Abstract*— Aiming at Unmanned Aerial Vehicle (UAV) swarm navigation in complex urban airspace, this paper proposes a virtual tube construction framework based on the Generalized Voronoi Diagram (GVD) skeleton. The framework employs the GVD to extract the medial skeletons of geometric environments at different altitude layers, thereby maximizing the utilization of clearance from obstacles. Through cross-layer topological associations, the planar topologies are upgraded and reconstructed into a global 3D navigation path, which then generates a continuous virtual tube space. Experimental results confirm that the proposed method achieves sub-millisecond planning speed while maintaining a safe clearance. Compared with traditional path planning algorithms, this method achieves a better balance between computational cost and environmental safety, effectively supporting real-time deployment of large-scale swarms.**

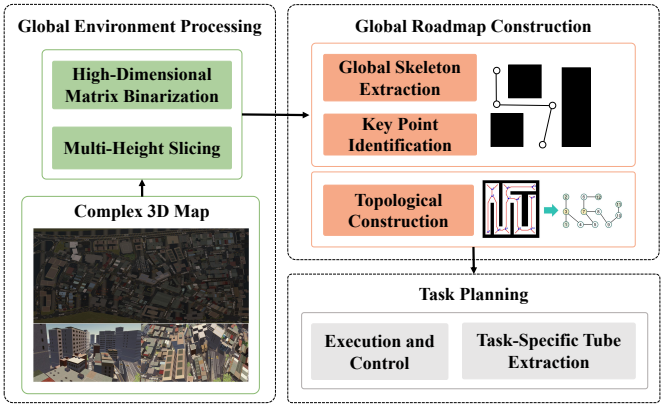


Fig. 1. Overview of the proposed skeleton-based virtual tube framework.

I. INTRODUCTION

With the deepening of urbanization and the maturation of electric Vertical Take-off and Landing aircraft technologies, Urban Air Mobility (UAM) is progressively emerging as a pivotal force for alleviating ground congestion and reshaping urban logistics and passenger transport paradigms [1], [2]. In the development of high-density UAM management systems, a core technical bottleneck for low-altitude digital infrastructure lies in achieving rapid global path allocation and real-time planning within 3D urban environments characterized by complex geometric constraints. Unlike 2D planar navigation or open-airspace flight, the urban low-altitude environment represents a typically constrained and unstructured space. Under traditional free-flight or simplistic point-to-point planning modes, aircraft operating in high-density, obstacle-rich urban areas face extreme collision risks and disordered competition, hindering large-scale deployment [3], [4]. As the density of Unmanned Aerial Vehicle (UAV) missions escalates, there is an urgent demand not only for local obstacle avoidance that satisfies kinematic constraints, but also for a global-view route guidance solution analogous to terrestrial road networks to optimize the allocation of spatial and temporal resources [5].

To ensure the safety and efficiency of UAM operations in low-altitude airspace, NASA introduced the concept of UAV Traffic Management, suggesting the use of multi-level geometric structures such as lanes, tubes, and corridors to guide UAV operations [6], [7]. Subsequently, the FAA further clarified the operational definition of UAM, advocating for the protection of flight safety through the delineation of specific 3D airspace volumes without traditional air traffic control intervention [8]. In the practical implementation of structured airspace, Professor Quan's team proposed the virtual tube concept, constructing digitized routes similar to ground vehicle lanes. This approach deeply couples global path planning with real-time local situational awareness, effectively partitioning flight areas and isolating building clusters and obstacles to guide large-scale swarms efficiently [9]. Utilizing distributed Vector Field methods, the team has designed various virtual tube scenarios including linear [10], curved [11], and circular [12] configurations and developed control algorithms to resolve the convergence and stability issues of tube traversal. To address complex geometric constraints in urban settings, such as narrow corridors, window frames, or portals, the Connected Quadrangle theory was proposed. This scheme deconstructs unstructured airspace into a series of continuous trapezoidal safety zones, achieving smooth swarm passage through constrained spaces via switching logic and gradient vector field control [13]. While existing research on virtual tubes has made significant progress in complex spatial control, challenges regarding efficiency and adaptability persist when constructing large-scale urban route networks. Currently, the generation of virtual tubes largely relies on a priori static paths or manually preset topologies. In complex 3D environments composed of high-density building clusters, the ability to automatically and rapidly map large-scale networks that meet both lane-width requirements and global efficiency objectives remains a critical hurdle for autonomous UAM operations.

This work was supported by the National Natural Science Foundation of China under Grant 62406345 and the Hunan Provincial Natural Science Foundation of China (2025JJ50341).

[1]Xunhua Dai is with the School of Computer Science and Engineering, Central South University, Changsha 410083, China (e-mail: dai.xh@csu.edu.cn).

[2]Yuting Liao is with the School of Electronic Information, Central South University, Changsha 410083, China (e-mail: liaoyt@csu.edu.cn).

As a prerequisite for constructing virtual tubes, the efficiency and precision of path planning methods directly determine the quality of the generated route network. Existing planning algorithms can be categorized into graph-based [14], sampling-based [15], potential field [16], and heuristic optimization [17] methods, depending on their spatial modeling and search mechanisms. Graph-based methods typically follow a dual-stage architecture from environment mapping to path searching, first discretizing continuous airspace into graph structures, such as voxel grids, and then utilizing Dijkstra or A* variants for optimization. Sparse A* Search improves traditional A* performance in 3D navigation by incorporating kinematic constraints [18], yet it remains highly dependent on fine discretization of free space. Consequently, computational complexity grows exponentially with increasing environmental scale and resolution, leading to the curse of dimensionality. Conversely, low-resolution grids may cause the loss of narrow-band paths, failing to meet UAM planning requirements in constrained airspace. For complex constrained environments, while RRT* algorithms can accelerate convergence in narrow spaces through strategies such as target tree construction, they still suffer from significant fluctuations in planning time and instability in path quality when ensuring continuous curvature and evading high-density obstacles [19]. As a geometric feature-based spatial decomposition method, the Voronoi diagram abstracts continuous 3D airspace into a lightweight topological skeleton by extracting geometric medial axes. This not only captures the essential structural characteristics of the environment but also significantly reduces the path search space [20], [21]. Unlike random sampling, Voronoi-based planning ensures that paths consistently maintain a safe distance from surrounding obstacles, thereby fundamentally mitigating collision risks.

This paper proposes a virtual tube construction framework guided by topological skeletons. The overall workflow is illustrated in Fig 1, and the main contributions are summarized as follows:

- A key node extraction method based on distance-angle constraints. To refine the environmental representation, a key point iterative completion mechanism is introduced to identify core intersections from the Generalized Voronoi Diagram (GVD) skeleton. This method significantly reduces the node scale of the topological graph while preserving the critical topological connectivity of complex urban airspace.
- A cross-dimensional reconstruction strategy from 2D slices to 3D topology. By deconstructing the 3D environment into multiple 2D layers and then reconstructing it using inter-layer association logic, the framework effectively avoids the curse of dimensionality and achieves fast path search in 3D space.
- A skeleton-guided virtual tube generation method. We implement a method that generates virtual tubes using topological skeletons. While maintaining a fixed minimum safety radius, the tube dynamically expands according to the local clearance, providing robust and scalable navigation for high-density swarm missions.

II. PROBLEM FORMULATION

To facilitate the construction of virtual tubes in complex urban environments, this section provides formal mathematical definitions for 3D environmental layering, virtual tubes, and topological construction.

A. Stratification of the 3D Environment

Consider a 3D urban airspace $\mathcal{W} \subset \mathbb{R}^3$ that contains a set of obstacles $\mathcal{O} = \{O_1, O_2, \ldots, O_m\}$. To facilitate computation, the continuous space is discretized into a 3D occupancy grid $\mathcal{M}$ with a resolution of δ. The occupancy state of any coordinate $p = (x, y, z) \in \mathcal{W}$ is represented by the following function:

$$\mathcal{M}(p) = \begin{cases} 1, & \text{if } \exists O_i \in \mathcal{O} \text{ s.t. } p \in \text{Interior}(O_i) \\ 0, & \text{otherwise} \end{cases} \tag{1}$$

To reconstruct the 3D space into a series of parallel 2D planar subtasks, we first discretize $\mathcal{M}$ along the vertical z-axis into multiple independent altitude layers with a uniform vertical spacing Δz, yielding a finite set $\mathcal{H} = \{h_1, h_2, \ldots, h_n\}$, as illustrated in Fig. 2. Each central altitude h_k corresponds to a vertical thickness interval $\left[h_k - \frac{\Delta z}{2}, h_k + \frac{\Delta z}{2}\right]$, within which a vertical downward maximum projection of the occupancy state is performed to obtain a tractable 2D plane $\mathcal{S}_{h_k} \subset \mathbb{R}^2$. For each $\mathcal{S}_{h_k}$, a clearance field is induced by the Euclidean Distance Transform (EDT), defined as $D(p) = \inf_{q \in \partial\mathcal{O}} \|p - q\|_2$, representing the proximity to the nearest obstacle boundary $\partial\mathcal{O}$.

The spatial discretization is governed by the grid resolution δ and altitude spacing Δz. The choice of δ balances efficiency and fidelity, typically set larger than the UAV's physical radius to ensure a conservative safety margin. Similarly, the altitude set $\mathcal{H}$ is determined by the environment's vertical complexity, where $\Delta z \geq 2 \cdot R(s)$ ensures a feasible volume. Specifically, non-uniform slicing is employed in obstacle-dense areas to capture topological details, while sparse slicing is used in open airspace to reduce the roadmap scale.

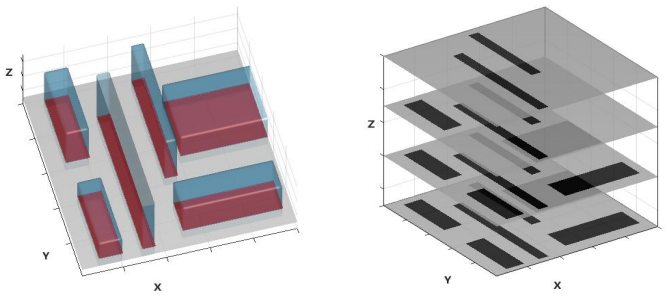


Fig. 2. Modeling and layering of the 3D spatial environment.

B. Virtual Tube Model

Let $\mathcal{C}_{free} \subseteq \mathcal{W} \setminus \mathcal{O}$ denote the collision-free configuration space. A virtual tube $\mathcal{T}$ is defined as a safe flight zone formed by radially expanding around the central axis curve $\sigma(s)$, where $\sigma(s) : [0,1] \to \mathcal{C}_{free}$ is a G^1 continuous curve. Assuming a tube radius function $R(s)$, its geometric space $\mathcal{V}_T$ can be described as the union of a cluster of spheres moving along the axis:

$$\mathcal{V}_T = \{p \in \mathbb{R}^3 \mid \exists s \in [0,1], \|p - \sigma(s)\|_2 \leq R(s) - \tau\} \quad (2)$$

To ensure that the constructed tube is safely passable in the physical environment, the construction of the tube must satisfy the following constraints:

$$R(s) + \tau \leq D(\sigma(s)), \forall s \in [0,1] \quad (3)$$

where $D(\cdot)$ represents the clearance field derived from the EDT, and τ is a safety margin factor ensuring the boundary condition $\partial\mathcal{V}_T \cap \mathcal{O} = \emptyset$.

C. Design Objectives of the Airway Network

The primary objective of this framework is to extract the airway network from the airspace and reconstruct it as a multi-layer directed graph $\mathcal{G} = (\mathcal{V}, \mathcal{E})$, so as to enable rapid planning and generation of virtual tubes. The multi-layer directed graph must satisfy the following conditions:

- Connectivity and Redundancy: The graph must accurately capture the essential connectivity of the free space $\mathcal{C}_{free}$, ensuring that the UAV swarm can find multiple reachable paths to avoid congestion.
- Safety Guaranteed Volume: Each edge in the graph supports the generation of a virtual tube. The tube maintains a fixed minimum radius for basic safety and expands its volume to utilize available clearance. This ensures a collision-free space that maximizes the separation from obstacles.
- Computational Efficiency: The graph must remain sparse to minimize the search space for path planning, enabling real-time spatial allocation and conflict resolution for high-density traffic.

III. PROPOSED METHODOLOGY

This section proposes a hierarchical virtual tube construction framework based on the GVD skeleton. By performing skeleton extraction and topological reconstruction on the environment, the framework reconstructs the complex airspace into a 3D topological graph, and further generates a smooth and continuous virtual tube navigation space.

A. Grid-Based GVD and Skeleton Extraction

Departing from classical Voronoi Diagrams restricted to point sets, the GVD generalizes spatial partitioning to accommodate complex geometric obstacles. Its primary strength is the ability to produce paths that maximize distance from obstacles, thereby yielding a navigation skeleton with superior safety margins for UAV swarms.

For any obstacle $\mathcal{O}_i$, its corresponding Voronoi region $\mathcal{V}_i$ is defined as the set of all points in the space that are closest to that obstacle. The union of the adjacent boundaries of the individual regions $\mathcal{V}_1, \mathcal{V}_2 ... \mathcal{V}_m$ constitutes the boundary surface $\mathcal{V}$ of the GVD. From the perspective of physical collision avoidance, any point p on $\mathcal{V}$ is equidistant to at least two different obstacles $\mathcal{O}_i, \mathcal{O}_j$. The set $\mathcal{V}$ of all such equidistant points is expressed as:

$$V = \{p \in C \mid \exists i \neq j, d(p, \mathcal{O}_i) = d(p, \mathcal{O}_j)\} \quad (4)$$

After obtaining the skeleton, identifying key feature points is the core step in topology construction. Skeleton feature points are classified as endpoints and branch points. Using 8-neighborhood scan to determine pixel types by analyzing the connectivity between the central pixel G_0 and its neighbors $G_i (i = 1, ..., 8)$. If there is only one foreground pixel, the point is classified as an endpoint. If there are at least three foreground pixels and the connectivity number is greater than 2, the point is classified as a branch point. The branch point set $\mathcal{B}$ is defined as the set of points where at least three Voronoi region boundaries intersect:

$$\mathcal{B} = \{p \in \mathcal{V} \mid \exists i \neq j \neq k,\ d(p, \mathcal{O}_i) = d(p, \mathcal{O}_j) = d(p, \mathcal{O}_k)\} \quad (5)$$

The 8-neighborhood method fails to detect high-curvature turns, as only branch intersections are recognized, leading to over-simplified paths. A distance and angle constrained key point extraction method is introduced.

For an identified pair of connected key points A and B, let P_{AB} be the set of discrete skeleton path points between them. Construct an auxiliary line l_{AB} and compute the perpendicular Euclidean distance d from each pixel on P_{AB} to this line. With a distance threshold $d_{threshold}$, the algorithm finds the point M with the maximum deviation. If $d > d_{threshold}$, M is marked as a potential key node candidate.

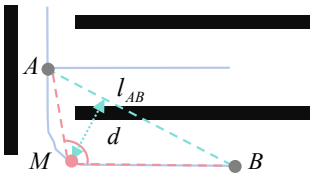


Fig. 3. Illustration of key point extraction.

To further ensure that this point has topological significance, the angle $\angle(A, M, B)$ formed by A, M, B is checked. M is formally confirmed as a new key point only if this angle is smaller than a preset threshold θ_{max}. As illustrated in Fig. 3, the blue line is the skeleton path, and point M is the extracted new key point. Split the path at M into P_{AM} and P_{MB}, recurse until all sub-path deviations are below the threshold or the angle condition fails.

B. Topological Reconstruction

When constructing topological relationships, the spatial connectivity between branch points is determined via skeleton path segments. Each segment is mapped to an edge $\mathcal{E}_k$ in the graph, forming a single-layer planar topological graph

$\mathcal{G} = (\mathcal{V}_k, \mathcal{E}_k)$. Isolated 2D topologies cannot fully represent the navigability of 3D airspace, so they are extended into an altitude-dependent multi-layer directed graph model.

The core of 3D reconstruction is to establish directed transition edges $\mathcal{E}_{inter}$ between feature node sets $\mathcal{B}_k$ and $\mathcal{B}_{k+1}$ of adjacent altitude layers. For a node $v_i^k \in \mathcal{B}_k$, vertical alignment is prioritized. If the horizontal projection distance $\|P(v_i^k) - P(v_j^{k+1})\|_2 \leq \epsilon_0$, a direct connection is made. Otherwise, a heuristic function $f(v_j^{k+1}) = \|P(v_i^k) - P(v_j^{k+1})\|_2 + \lambda \cdot \Delta z$ searches for the optimal match. Inter-layer directed edges are defined as:

$$\mathcal{E}_{inter} = \left\{ (v_i^k, v_j^{k+1}) \middle| \begin{matrix} \|\mathcal{P}(v_i^k - v_j^{k+1})\|_2 \leq \delta \\ l(v_i^k, v_j^{k+1}) \cap \mathcal{O}_{3D} = \emptyset \end{matrix} \right\} \quad (6)$$

This hierarchical reconstruction framework successfully transforms the path retrieval problem from $O(N^3)$ in the original 3D space into a search task on a sparse skeleton network. The computational complexity is reduced to $O(N_k \cdot |B_k|^2)$.

C. Obtaining the Curve for Tube Generation

To perform fast global planning in the pre-constructed skeleton topological network and obtain the generated curve of the tube, the first issue to address is how to connect the start point p_s and the goal point p_g. Typically, p_s and p_g do not lie exactly on the skeleton. Directly connecting them to the nearest skeleton nodes often forces detours or creates sharp turning angles, thereby increasing total flight distance and burden. Inspired by [22], a connection strategy based on distance equivalence constraints is proposed to obtain shorter and more natural connection paths.

Specifically, p_s is treated as a hypothetical obstacle, build $\hat{\mathcal{O}} = \mathcal{O}_{obs} \cup p_s$, , and find candidate access set $\mathcal{V}_s$:

$$\forall p_j \in \mathcal{V}_s, \quad d(p_j, p_s) = d(p_j, \mathcal{O}_{obs}) \quad (7)$$

Similarly, for the goal point p_g, the set $\mathcal{V}_g$ can be determined. After computing the access points, p_s, p_g and their corresponding candidate sets $\mathcal{V}_s, \mathcal{V}_g$ are temporarily incorporated into the topological graph. Then, a search algorithm is used to obtain the optimal node sequence $P_{ref} = \{p_s, v_1, v_2, \ldots, p_g\}$. A piecewise B-spline is adopted to smooth the skeleton sequence, and $\sigma(s)$ is expressed as a k-order piecewise polynomial function. The skeleton sequence is sparsely sampled at equal intervals to extract a set of control points $Q = \{q_0, q_1, \ldots, p_m\}$ representing the geometric characteristics of the environment.

When processing high-curvature turns, B-spline fitting often produces corner-cutting artifacts, causing the curve to shift toward the interior side of obstacles. To address this, the local deviation between the fitted curve $\sigma(s)$ and its corresponding original skeleton point v_j must be constrained within the local safety radius $R_{gvd}(v_j)$ derived from the GVD:

$$\forall v_j \in P_{\text{ref}}, \quad \|\sigma(s_j) - v_j\|_2 \leq \alpha \cdot R_{gvd}(v_j) \quad (8)$$

where $\alpha \in [0, 1]$ is a centripetal factor. When α is small, the curve is forced to stay close to the skeleton, thereby strictly ensuring the curve is collision-free while maintaining flight smoothness.

IV. Simulation

A. Comparison on Path Searching

The generation quality of the baseline curves directly determines the safety of the generated virtual corridors. Two representative search algorithms, A* and RRT, are selected as baselines to evaluate the planning efficiency and quality of the generated curves under three types of 2D maps: maze, geometric, and irregular maps. In this section, the Dijkstra algorithm is adopted to determine the optimal path on the constructed topological graph. It should be noted that Dijkstra is used only as a representative search method for validating planning performance.

For the quality of the planned pipeline generation lines, three metrics are defined for comparison: planning time T_c, minimum safe clearance $C_{\min}$, and path length L. Path length L is directly related to flight range and mission execution time. Planning time T_c is crucial for drone swarm tasks with high real-time requirements. Minimum safe clearance $C_{\min}$ is defined as the minimum Euclidean distance from a path point to the nearest obstacle boundary. Given the same start point and target point, the performance comparison of path planning between the proposed algorithm and the two baseline algorithms under three types of maps is shown in Tables I and Table II. Our method demonstrates a decisive advantage in computational speed across all test maps.

TABLE I

Comparison of execution time of path planning algorithms under different map types

Map Type	Proposed method (s)	A* (s)	RRT (s)
Geometric	**0.0008 s**	0.0064 s	0.0056 s
Maze	**0.0007 s**	0.0063 s	0.0935 s
Irregular	**0.0004 s**	0.0022 s	0.0051 s

TABLE II

Comparison of quality metrics of path planning algorithms under different map types

Map Type	L (m)			$C_{\min}$ (m)		
	Proposed	A*	RRT	Proposed	A*	RRT
Geometric	75.31	**57.87**	69.26	**7.16**	0.5	1.8
Maze	241.01	**206.98**	277.96	**6.71**	1.0	2.0
Irregular	92.52	**80.56**	93.89	**3.61**	1.0	1.0

To further validate the effectiveness of the proposed method in sequential multi-task waypoint planning, we preset 10 fixed target points in a maze map scenario, and the simulation results are illustrated in Fig. 4. The visiting path generated by the proposed method exhibits a more regular topological structure in spatial distribution. In contrast, this path not only maintains a high level of route regularity but

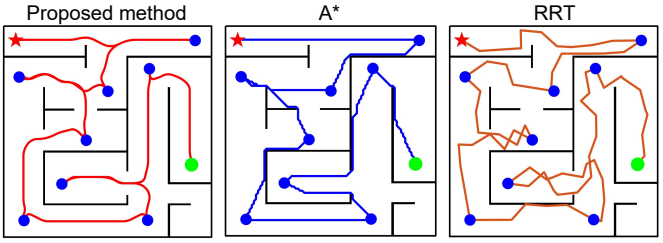


Fig. 4. Comparison of different algorithms for ten-waypoint path planning.

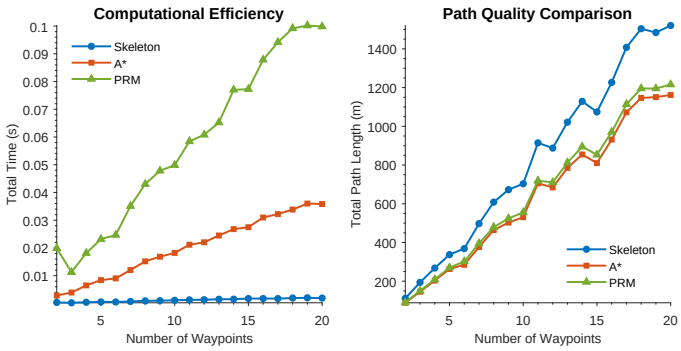


Fig. 5. Performance comparison of different path planning algorithms.

also demonstrates superior logical connectivity during multi-target switching.

Through 20 independent simulation trials, the performance of the proposed algorithm is compared with that of A* and PRM in path planning scenarios with varying numbers of target points. A fixed-target-point strategy is adopted, with the number of points increasing from 1 to 20, focusing primarily on computational time and path length. As illustrated in Fig. 5, as mission complexity increases, the execution time of RRT rises sharply, while the time consumed by the skeleton-based extraction method remains nearly constant and is the lowest among all methods. Thanks to the one-time offline construction of the skeleton topological graph, only task-oriented path extraction is required in the online phase, eliminating the need for repeated re-sampling of the 3D space. The total path length generated by the proposed method is higher than that of A* and PRM. Although it does not offer an advantage in shortest distance, this cost is a deliberate trade-off for airspace order and safety. The generated planning path consistently follows the medial axis of the free space, maximizing the safe clearance from obstacles.

B. Simulation For Swarm Flying

To evaluate the operational stability of the proposed framework, a swarm mission involving 10 UAVs is conducted in environment. We implement an Artificial Potential Field (APF) based control law for decentralized obstacle avoidance and inter-agent separation. The performance is compared between two guidance paradigms: the proposed virtual tube-constrained guidance and the traditional inflated A* path guidance. The swarm is initialized at a common starting point, and the mission objective is to navigate through narrow passages to reach the destination.

As illustrated in Fig. 6, the simulation results demonstrate that the most significant advantage of the proposed framework lies in the provision of superior safety margins for the swarm. The A* algorithm, driven by heuristic cost minimization, tends to generate paths that closely follow the boundaries of obstacle clusters. Even with pre-defined inflation, this proximity severely limits the available space for the APF-based reactive control. When agents perform high-speed maneuvers or inter-agent separation, they are frequently pushed toward the obstacle boundaries, leaving minimal room for error or emergency collision avoidance.

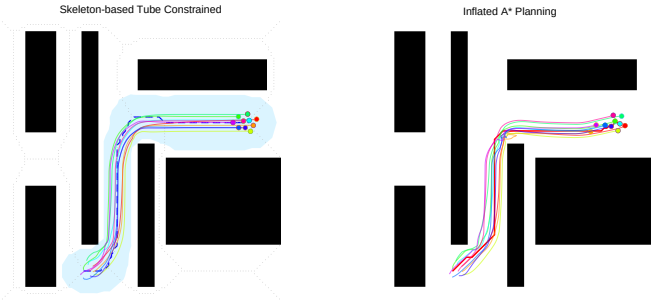


Fig. 6. Comparative simulation of swarm navigation using the proposed virtual tube framework versus inflated A* path planning.

In contrast, the virtual tube derived from the GVD inherently occupies the medial axis of the free space. By maintaining a centralized guidance curve $\sigma(s)$, the framework provides the swarm with a significantly broader safety buffer on both sides of the path. This additional spatial resource is crucial during cornering and obstacle avoidance phases, as it allows the agents to execute separation maneuvers without approaching the building structures.

C. 3D Topological Planning and Inter-layer Navigation

This set of experiments aims to validate the topological reconstruction performance of the proposed framework in complex 3D environments with significant height variations. The start layer $h_{start} = 20$m and the target $h_{goal} = 35$m are selected for a cross-layer task.

Fig. 7 illustrates the key topological nodes of the 2D skeletons obtained via projection at the two height layers. These nodes serve as the geometric foundation for cross-layer connections. Climbing segments are constructed according to an inter-layer interconnection strategy that prioritizes vertical alignment and supplements with heuristic matching.

As illustrated in Fig. 8, the generated curve is obtained through global path planning on the reconstructed 3D skeleton. A tube region with a radius of 2m is constructed and used as a spatial constraint to guide the UAV flight. A UAV is simulated to traverse the tube, with its control method as described in subsection IV-B. The total flight path length is 187.41m. Experimental results show that even in a complex environment with a height span of up to 15m, the planned flight trajectory of the UAV is strictly confined

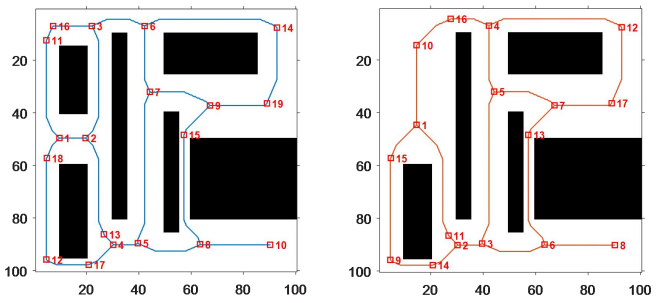


Fig. 7. Skeleton extraction and topological keypoint construction at 20 m and 35 m altitude layers.

within the tube space, verifying the effectiveness of the proposed topological scheme in handling complex 3D spaces.

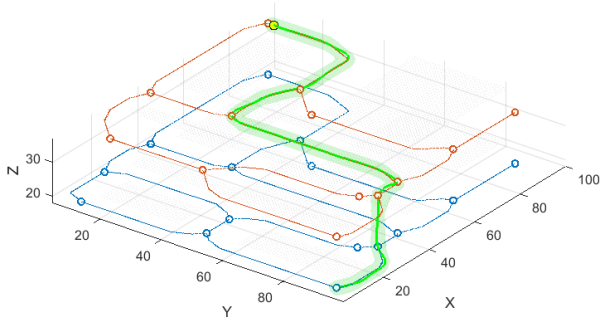


Fig. 8. Trajectory Planning Constrained by 3D Virtual Tubes.

V. Conclusion

This study proposes a hierarchical virtual tube construction framework based on the GVD skeleton to enable safe UAV swarm navigation in complex urban environments. The framework decomposes the 3D airspace into multiple 2D layers via vertical stratified sampling, significantly reducing path planning complexity. The GVD algorithm extracts the medial-axis skeleton of free space in each layer, and an iterative completion mechanism with distance-angle constraints is introduced for environment-aware keypoint extraction and topological mapping. Cross-layer association then integrates local 2D skeletons into a global 3D topological graph, generating guidance curves and virtual tubes with spatiotemporal continuity and high safety margins. Experimental results show an order-of-magnitude improvement in computational efficiency over A* and RRT, providing a topologically guaranteed hard-constrained space for high-density swarm planning.

Future work may extend this framework to dynamic environments by developing a local topological state update mechanism to enable real-time responses to moving obstacles or temporary no-fly zones.

References

[1] H. Liu, G. Wu, L. Zhou, W. Pedrycz, and P. N. Suganthan, "Tangent-based path planning for UAV in a 3D low altitude urban environment," IEEE Trans. Intell. Transp. Syst., vol. 24, no. 11, pp. 12062–12077, Nov. 2023.

[2] S. G. Manyam, D. W. Casbeer, S. Darbha, I. E. Weintraub, and K. Kalyanam, "Path planning and energy management of hybrid air vehicles for urban air mobility," IEEE Robot. Autom. Lett., vol. 7, no. 4, pp. 10176–10183, Oct. 2022.

[3] J. Cho and S. Choi, "Toward safe integration of UAM in terminal airspace: UAM route feasibility assessment using probabilistic aircraft trajectory prediction," IEEE Trans. Intell. Transp. Syst., in press.

[4] P. Wu, et al., "Risk-bounded and fairness-aware path planning for urban air mobility operations under uncertainty," Aerosp. Sci. Technol., vol. 127, p. 107738, 2022.

[5] M. C. R. Murça, "Identification and prediction of urban airspace availability for emerging air mobility operations," Transp. Res. Part C: Emerg. Technol., vol. 131, p. 103274, 2021.

[6] P. Kopardekar, et al., "Unmanned aircraft system traffic management (UTM) concept of operations," in 16th AIAA Aviat. Technol. Integr. Oper. Conf., Washington, D.C., USA, 2016.

[7] J. Lieb and A. Volkert, "Unmanned aircraft systems traffic management: A comparsion on the FAA UTM and the European CORUS ConOps based on U-space," in Proc. 39th Digit. Avionics Syst. Conf. (DASC), San Antonio, TX, USA, 2020, pp. 1–6.

[8] Federal Aviation Administration, "Urban air mobility (UAM) concept of operations v2.0," Washington, D.C., USA, FAA, April 26, 2023.

[9] P. Mao and Q. Quan, "Making robotics swarm flow more smoothly: A regular virtual tube model," in Proc. IEEE/RSJ Int. Conf. Intell. Robots Syst. (IROS), Kyoto, Japan, 2022, pp. 4498–4504.

[10] Q. Quan, R. Fu, M. Li, D. Wei, Y. Gao, and K. -Y. Cai, "Practical distributed control for VTOL UAVs to pass a virtual tube," IEEE Trans. Intell. Veh., vol. 7, no. 2, pp. 342–353, June 2022.

[11] Q. Quan, Y. Gao, and C. Bai, "Distributed control for a robotic swarm to pass through a curve virtual tube," Robot. Auton. Syst., vol. 162, p. 104368, 2023.

[12] Y. Gao, et al., "Multi-UAV cooperative target encirclement within an annular virtual tube," Aerosp. Sci. Technol., vol. 128, p. 107800, 2022.

[13] Y. Gao, C. Bai, and Q. Quan, "Distributed control for a multiagent system to pass through a connected quadrangle virtual tube," IEEE Trans. Control Netw. Syst., vol. 10, no. 2, pp. 693–705, June 2023.

[14] J. Park, I. Jang, and H. J. Kim, "Decentralized deadlock-free trajectory planning for quadrotor swarm in obstacle-rich environments," in Proc. IEEE Int. Conf. Robot. Autom. (ICRA), London, UK, 2023, pp. 1428–1434.

[15] I. B. Jeong, S. J. Lee, and J. H. Kim, "Quick-RRT*: Triangular inequality-based implementation of RRT* with improved initial solution and convergence rate," Expert Syst. Appl., vol. 123, pp. 82–90, 2019.

[16] Y. Rasekhipour, A. Khajepour, S. -K. Chen, and B. Litkouhi, "A potential field-based model predictive path-planning controller for autonomous road vehicles," IEEE Trans. Intell. Transp. Syst., vol. 18, no. 5, pp. 1255–1267, May 2017.

[17] R. Xu, Z. Huang, C. Wang, and H. Yan, "Evolving collaborative differential evolution for dynamic multi-objective UAV path planning," IEEE Trans. Veh. Technol., in press.

[18] G. Xu, et al., "Hierarchical trajectory planning for multi-UAVs via sparse A* search and linear programming," in Proc. Int. Conf. Guidance, Navig. Control, Singapore, 2022.

[19] M. Kim, J. Ahn, and J. Park, "TargetTree-RRT*: Continuous-curvature path planning algorithm for autonomous parking in complex environments," IEEE Trans. Autom. Sci. Eng., vol. 21, no. 1, pp. 606–617, Jan. 2024.

[20] H. Niu, X. Ji, L. Zhang, F. Wen, R. Ying, and P. Liu, "A skeleton-based topological planner for exploration in complex unknown environments," in Proc. IEEE Int. Conf. Robot. Autom. (ICRA), Atlanta, GA, USA, 2025, pp. 11766–11772.

[21] J. Wen, X. Zhang, Q. Bi, H. Liu, J. Yuan, and Y. Fang, "G^{2}VD planner: Efficient motion planning with grid-based generalized Voronoi diagrams," IEEE Trans. Autom. Sci. Eng., vol. 22, pp. 3743–3755, 2025.

[22] M. R. H. Al-Dahhan and K. W. Schmidt, "Voronoi Boundary Visibility for Efficient Path Planning," IEEE Access, vol. 8, pp. 134764–134781, 2020.